Improving Carbon Nanotube Composites Through Interface Control *via* Polymer Grafting

Won Jun Lee,[a, b, 1] Adam J. Clancy,[a, c, 1] Juan C. Fernández-Toribio,[d, e] David B. Anthony,[a] Edward R. White,[a] Eduardo Solano,[f] Hannah S. Leese,[a, g] Juan J. Vilatela,[e] Milo S. P. Shaffer[a, h, *]

[a] Department of Chemistry, Imperial College London, London, SW7 2AZ, United Kingdom
[b] Department of Fiber System Engineering, Dankook University, Yongin, 16890, Republic of Korea
[c] Department of Chemistry, University College London, London, WC1E 6BT, United Kingdom
[d] Department of Materials, Science Polytechnic University of Madrid, 28040, Madrid, Spain
[e] IMDEA Materials Institute, Eric Kandel, 2, Tecnogetafe, 28906, Getafe, Madrid, Spain
[f] NCD-SWEET beamline, ALBA synchrotron light source, 08290 Cerdanyola del Vallès, Barcelona, Spain
[g] Department of Chemical Engineering, University of Bath, Bath BA2 7AY, United Kingdom
[h] Department of Materials, Imperial College London, London, SW7 2AZ, United Kingdom

Abstract

Nanocomposites are critically influenced by interfacial interactions between the reinforcement and matrix. Single-walled carbon nanotubes (SWCNTs) were grafted with polyvinyl alcohol (PVOH) of varying molecular weights, to improve the interfacial interaction with a homopolymer PVOH matrix. Nanocomposite fibers were coagulation spun across a broad range of loading fractions, controlled by the spinning dope composition. An intermediate grafted-PVOH molecular weight (10 kDa) maximized grafting ratio, and the final composite mechanical performance; the positive effects were attributed to the increased degree of dispersion of the SWCNTs in the dope, as well as the favorable interface. The PVOH grafting stabilized increased SWCNT loading fractions (up to 45 wt.%), offering increased strength (up to 1100 MPa) and stiffness (up to 38.5 GPa); at the same time, strain-to-failures remained high (up to 23.3%), resulting in high toughness (up to 125 J g^{-1}).

[*] Corresponding author. E-mail: m.shaffer@imperial.ac.uk (Milo S. P. Shaffer), +44 (0) 2075945825

[1] These authors contributed equally.

1. Introduction

Classic fiber reinforced composites, in particular carbon and glass systems, use continuous fibers in a brittle matrix to exploit the excellent uniaxial strength and stiffness of the constituents [1]. However, application is often limited by a low ultimate strains and the lack of plastic deformation before catastrophic failure [2]. While recent advances in composite layup (use of hybrid composites [3] or thin plies [4]) has recently been shown to introduce pseudo-ductility, fully ductile composites require fundamentally ductile components to replace the conventional brittle constituents. While high strength, tough polymers are well established, there is clearly a need for a high performance ductile fiber which maintains high strength and stiffness [5].

Single-walled carbon nanotubes (SWCNTs) offer exceptional intrinsic strength, stiffness, and toughness, as well as high thermal and electrical conductivities, all at low density [6, 7]. They have been widely explored as high performance (multifunctional) reinforcements for a range of matrices, particularly polymers. Their high aspect ratio and anisotropic properties make them particularly suited to nanocomposite fiber applications [8-10]. One strategy is to form ‘yarns’ directly from pure, dry, entangled nanotubes, either by drawing ‘forests’ grown on a substrate [11], or by spinning gas-phase networks or aerogels formed in the reactor during chemical vapor deposition [12-14]. These yarns can be subsequently infiltrated with resin to form composites fibers [15-17]. Whilst dry routes are appealing, they are necessarily linked to the synthesis, limiting the types of SWCNTs that can be used and the opportunities for purification or functionalization of the interfaces. Liquid or melt phase spinning of pre-grown SWCNT powders to form nanocomposite fibers offers greater flexibility and potentially simple upscaling using conventional technology. One significant challenge is that nanotube-nanotube van de Waals interactions [18] tend to drive SWCNTs to form rope-like bundles [19], with a poor shear strength. Poorly exfoliated bundles have reduced SWCNT-matrix interfacial area, and slip internally under load [20], limiting their load-carrying ability [21]; they may also act as defects or stress-concentrations initiating premature failure. Agglomerates become more prevalent at higher loading fractions, so while increasing the SWCNT loading in a composite initially increases mechanical properties, the degree of agglomeration begins to dominate even at moderate (<5 wt.%) loadings, eventually reducing bulk mechanical performance [22].

Melt spinning routes tend to be limited to less than approximately 10 wt.% carbon nanotubes due to viscosity and wetting limitations [9, 23]. Instead, composite fibers may be

produced by coagulation wet-spinning of a SWCNT dope injected into a (co-flowing) anti-solvent. Use of a pure SWCNT solution forms a wet-spun nanotube yarn [24, 25], while use of a polymer solution as anti-solvent has been used to form nanocomposite fibers. Polyvinyl alcohol (PVOH) is the most common matrix used for SWCNT coagulation spinning, for both convenience and performance [9, 10]. Post-processing, by hot-drawing, dramatically increases PVOH crystallinity, improving properties, and diminishing water sensitivity.

The degree of agglomeration in wet-spun composite fibers can be linked to the degree of exfoliation in the dope. SWCNTs may be fully debundled as individualized solubilized species through the use of reductive chemistry [26] or superacids [24]. Although they have shown promise in the synthesis of high toughness, cross-linked composites [27, 28], the inherent high reactivity and air/water sensitivity of reduced nanotubes complicates their application. Superacid solutions have not yet been used in composite manufacture, likely owing to the incompatibility of the highly corrosive and dehydrating acids with potential matrices. Instead, most SWCNT dispersions used for spinning are metastable and are formed through high shear techniques, commonly (ultra)sonication. However, without the addition of a stabilizing additive (adsorbed surfactant or polymer), pristine SWCNTs quickly reagglomerate. Unfortunately, these stabilizing species typically remain in the final fibers, limiting interfacial stress transfer and hence the overall mechanical performance. SWCNTs can be dispersed in low volatility amides, but these solvents are difficult to remove and can act as plasticizers, again compromising composite strength [29].

Covalent functionalization of the SWCNTs [30] can improve dispersibility without addition of a mobile stabilizer, while also providing an opportunity to strengthen the SWCNT-matrix interface [31, 32]. Polymer grafting, in particular, offers steric stabilization in solution and a potentially, strong, interdiffused interface [33]. In *graft-from* methods, the polymer is grown in situ from the nanotube surface [34], whereas *graft-to* methods attach well-defined, pre-synthesized polymers [35, 36]. The *graft-from* approach facilitates higher grafting ratios (weight fraction of grafted polymer relative to the SWCNT framework), but the molecular weight remains unknown. In *graft-to* reactions, the grafting ratio initially increases with molecular weight; however, at higher molecular weights, grafting ratio decreases due to the steric bulk of larger polymers. Intermediate molecular weights, therefore, maximize the grafting ratio and hence dispersibility [37].

Here, we prepare well-defined PVOHs, of varying molecular weight, for *graft-to* functionalization of SWCNTs (f-SWCNTs). The intention was that the f-SWCNTs would form stable dispersions, at relatively high concentrations, including in the presence of homopolymer PVOH, to generate dopes for coagulation spinning. In contrast to systems in which the homopolymer diffuses from the coagulant, the microstructure should be more uniform, with a defined minimum spacing between the well-exfoliated SWCNTs. At the same time, the grafted PVOH is expected to be miscible with bulk matrix PVOH, maximizing interfacial interactions, and improving the (nano)composite fiber performance.

2. Experimental

2.1 Materials

Tuball SWCNTs (Lot # 4-18032014) were purchased from OCSiAl LLC (LU). Acetic acid (>99.8%), 2,2′-azobis(2-methylpropionitrile) (98%), N,N-dimethylacetamide (DMAc, anhydrous, 99.8%), di-t-butyl dicarbonate (>99%), ethanol (anhydrous >99.5%), lauroyl peroxide (Luperox® LP, 97%), naphthalene (99%), potassium O-ethyl xanthate (98%), PVOH (Mowiol® 4-88, M_w ~31,000), pyridine (anhydrous, 99.8%), sodium (ingot, 99.99%), sodium azide (>99.5%), sodium nitrite (99.999%), thionyl chloride (>99%), trifluoroacetic acid (99%), dimethyl sulfoxide (DMSO, >99.9%), and vinyl acetate (>99% with 3-20 ppm hydroquinone stabilizer) were purchased from Sigma Aldrich (GB). Acetone (99.9%), dichloromethane (DCM, 99.9%), ethanol (96%), n-hexane (99.9%), isopropyl alcohol (99.9%), petroleum benzine (petrol, 40-60 °C fraction), sodium sulphate (>99%), sodium hydrogen carbonate (>98%), sodium hydroxide (99.9%), and tetrahydrofuran (THF, 99.9%) were purchased from VWR UK Ltd. (GB), and 4-aminobenzylalcohol (98 %) was purchased from Fluorochem Ltd. (GB).

2.2 Characterization

Scanning electron microscopy (SEM) micrographs were taken with a LEO Gemini 1525 field emission gun SEM (Carl Zeiss AG, DE) controlled by Smart SEM software, with a working distance of ca. 7 mm, accelerating voltage of 10 keV, and a 30 μm aperture using an InLens detector. As-received materials were adhered using silver dag (Agar Scientific Ltd., GB). Dilute dispersions were drop-cast on aluminum foil covered stubs and were dried in ambient conditions. The dried samples were then submerged in deionized water and

tetrahydrofuran briefly to remove NaOH and naphthalene, before drying in ambient conditions.

High-resolution Transmission electron microscopy (TEM) images were taken with an aberration-corrected FEI Titan operated at 80 kV and additional TEM images were carried out on a JEOL2100Plus TEM at 200 kV. A dilute (f-)SWCNT/ethanol suspension was drop cast onto a holey carbon film on a 200 mesh copper grid (Agar Scientific Ltd., GB), and left to dry at room temperature.

Thermogravimetric analysis (TGA) was performed on a TGA/DSC 1 (Mettler Toledo International Inc., CH), with a GC200 flow controller, using STARe software v12.00C. The samples were heated under nitrogen from 30 °C to 100 °C at 35 °C min^{-1}, then held isothermally at 100 °C for 30 min to dry, and the temperature ramped to 750 °C at 10 °C min^{-1}.

SWCNT-reinforced composite fiber samples were prepared and tested based on the standard ISO BSI11566 for single carbon fibers. The tensile specimens were mounted on a card template (15 mm gauge) using an epoxy adhesive (Araldite Rapid, Huntsman Corporation, US) to aid handling. Samples were tested using a TST350 Tensile Stress Tester (Linkam Scientific Ltd., GB) fitted with a 20 N loading cell. Samples were measured with a cross head displacement rate of 16 μm s^{-1} until failure. Fiber cross-sectional areas were taken from SEM fracture surfaces (true stress); fiber diameter is assumed to be circular, as supported by cross-sectional SEM. Tensile modulus was determined from linear regions between 0.1 to 0.6% strain.

Raman spectroscopy was performed on a Renishaw InVia micro-Raman Spectrometer (Renishaw Plc., GB) using a 532 nm (32 mW, 10% power) laser with 1800 line/mm grating, centered around 2050 cm^{-1}. A high laser power was required due to significant attenuation during the different polarization configurations. Raman mapping was performed through iterative point spectra collected from 360 points (30×12) in a ~300 μm^2 array with a 5 s acquisition time for each point. Polarized Raman was performed through manual introduction of half waves plates between incident light source/sample, and sample/detector.

Small- and wide-angle two-dimensional X-ray scattering (SAXS and WAXS, respectively) patterns were obtained at NCD-SWEET beamline at ALBA synchrotron light source, ES. A monochromatic beam with wavelength of 0.998 Å was selected using a Si (111) double crystal monochromator. The beam size at the sample position was ca. 100 × 50 μm^2 (H × V,

FWHM). The SAXS detector was a Pilatus3S 1M (Dectris®) which consists of an array of 981×1043 pixels (H × V) with a pixel size of 172 × 172 μm^2. The calibration of the wavevector scale of the scattering curve was calculated using Silver Behenate. Complementary WAXS patterns were collected using a LX255-HS area detector from Rayonix®, which consists of a pixel array of 1920 × 5760 (H × V) with a pixel size of 44 × 44 μm^2. The wavenumber $q = 4\pi/\lambda \sin\theta$ scale for WAXS experiments scale calibration was achieved by using Cr_2O_3 as calibrant. Data were processed with the software Data Analysis WorkbeNch (DAWN) [38]. Azimuthal profiles were obtained by radial integration after background subtraction. The degree of orientation of SWCNT was quantified from the full-width-at-half-maximum (FWHM) of the azimuthal intensity distribution (fitted as Lorentzian functions) across the *q* range analyzed (0.01-0.025 $Å^{-1}$), subtracting the constant intensity contribution to the azimuthal profiles.

Differential scanning calorimetry (DSC, 204 F1 Phoenix®, Netzsch, DE) thermal analysis was used to determine the PVOH crystallinity in the drawn fibers. Samples were analyzed in a nitrogen atmosphere and cycled twice from 35 ºC to 250 ºC at a heating rate and cooling rate of 10 ºC min^{-1}. The two endothermic peaks for melting and decomposition temperatures overlapped for PVOH. Overlapped peaks were thus deconvoluted by peak fitting a bi-Gaussian peak for melting and a Gaussian peak for decomposition around the two specified temperatures (ca. 225 ºC and 233 ºC for melting and decomposition temperatures, respectively). The integration of the melting peak areas, normalized to the percentage total PVOH in the sample, and the melting enthalpy was compared to pure crystalline PVOH (156 J g^{-1}**)** [39] to determine the degree of crystallinity.

2.3 Procedures

Acyl-protected polyvinyl acetate (PVAc) synthesis was performed as reported in Clancy *et al* [27]. In short, the reversible addition–fragmentation chain transfer (RAFT) agent S-(4-((t-butoxycarbonyl)amino)benzyl)-O-ethyl xanthate was synthesized from 4-amino benzyl alcohol through Boc protection of the amine and conversion of the hydroxyl to an O-ethyl xanthate *via* an alkyl chloride formed through treatment with thionyl chloride, followed by metathesis with the potassium xanthate salt. Neat vinyl acetate was subsequently polymerized, using varying equivalents relative to the RAFT agent to control molecular weight. The xanthate was removed with benzoyl peroxide, the amine deprotected with triflouroacetic acid, and the amine converted to azide *via in situ* diazonium formation using

sodium nitrite and sodium azide. SWCNTs were purified reductively according to a previously reported procedure [40]. In short, under inert atmosphere, dried SWCNT powder was soaked in 1 mL $mg_{(SWCNT)}^{-1}$ DMAc with 0.1 eq of sodium and naphthalene for 48 h before centrifugation (1,000 g, 30 min) to separate dissolved impurities from the pure SWCNT sediment.

Functionalization of SWCNTs with azide-terminated PVAc was adapted from Qin *et al* [41]. Purified SWCNTs (6 mg, 0.5 mmol, 1 eq) were added to anhydrous DMAc (45 mL) and bath sonicated (75 W, 30 min). The azide terminated polymer (0.033 eq) was dissolved in 5 mL DMAc and added to the SWCNT dispersion. The mixture was heated to 140 °C for 72 h before cooling to room temperature and filtering through a 100 nm polytetrafluoroethylene (PTFE) membrane. Before drying on the filter membrane, the wet-cake was mixed with DMAc (100 mL) sonicated and filtered to remove non-grafted PVAc. This procedure was repeated with tetrahydrofuran before drying at room temperature overnight to give the f-SWCNTs. SWCNTs functionalized with PVAc were deacetylated by soaking in saturated potassium hydroxide methanol solution for 30 min, before filtering and washing with methanol and allowed to dry at room temperature overnight to give f-SWCNTs [42].

Spinning dopes were prepared with a constant total solids content (PVOH and f-SWCNT) of 40 mg mL^{-1} (total volume varied between 4 and 16 mL) in a 3:1 v/v DMSO/water mixture. The loading of SWCNT (excluding the weight of the grafted polymer) was varied between 0-60 wt.% relative to the polymer fraction (compromising the grafted PVOH and the free PVOH (Mowiol®)). Functionalized-SWCNTs were dispersed in the water component through probe sonication (5 min, tip sonicator, 150 W) before dropwise addition to a homopolymer PVOH/DMSO stock solution, with stirring. The mixture was briefly sonicated (5 min, 150 W) again and passed through a syringe filter (PTFE, 200 μm) to remove residual macroscopic agglomerations.

Fibers were spun through injection into a rotating bath of acetone, used as coagulant. Injection was performed at 10 mL s^{-1} through a 21-gauge cannula (i.e. 0.8 cm s^{-1}, stainless-steel, Central Surgical Co. Ltd., GB) using a syringe pump (KDS100, KD Scientific, US), while the bath was rotated at 2.0 cm s^{-1} at the point of injection to provide extensional flow during fiber coagulation. The fibers were soaked for 1 h and then removed from acetone, wound about a circular glass vial and stored in a saturated humidity atmosphere, relative humidity 70%, until post-processing.

Post-processing of the fibers was performed with on a micro fiber conditioning line (DSM Xplore Fiber Conditioning Unit, NL) with varying draw ratio (1.8 for composites, 2.0 for pure PVOH) and a furnace temperature of 180 °C.

3. Results and discussion

3.1 Grafting PVOH to SWCNT

The functionalizing polymers were synthesized by RAFT polymerization, as developed previously [37]. The RAFT route allows fine control over polymer molecular weight with a low polydispersity, while enabling independently controllable end groups: here, a terminal azide and hydrogen. Four different polymer molecular weights were synthesized (5, 10, 30, and 60 kDa) and grafted onto the SWCNTs. Due to the incompatibility of the hydroxyl side groups with both RAFT polymerization and SWCNT grafting conditions, the functionalization was performed with the acetylated polymer (PVAc).

The azide-terminated PVAc was grafted onto ultrasonically-dispersed SWCNTs forming an aziridine link with the SWCNT surface, via established chemistry [37]. Tuball SWCNTs were selected for their high crystallinity, and low cost, consistent with composite applications; the SWCNTs were purified using reductive purification before use [43]. After functionalization, the polymer backbone was subsequently deacetylated with potassium hydroxide and methanol through base hydrolysis to give the PVOH f-SWCNTs [42].

The grafting stoichiometry (C/R, SWCNT carbons per polymer chain, estimated using the number average molar mass, M_n) and grafting ratio (weight of grafted polymer as a percentage of SWCNT weight) follow established trends with polymer molecular weight (Figure 1a). The C/R increases with molecular weight as increasing steric occlusion on the nanotube surface increases the distance between grafting sites. Relatedly, the grafting ratio follows a non-linear trend, increasing at low molecular weights due to increasing per-polymer weight, up to 29 wt.% for 30 kDa, before decreasing at higher molecular weights as steric occlusion dominates (Supplementary Figure S1a). TEM of the 10 kDa f-SWCNT (Figure 1b) shows a core (SWCNT)-shell (PVOH) structure, absent in the as-received or purified SWCNTs (Supplementary Figure S2), indicating successful grafting.

The f-PVOH dramatically improves the dispersibility of SWCNTs in the dope solvent (DMSO/water mixture), as clearly shown by optical microscopy (Figure 1e-g), while unfunctionalized SWCNTs failed to disperse (Figure 1d), remaining as aggregates 10’s of

microns across. There appears to be some dilute segregation of f-SWNT which gradually disappears with increasing chain length from 5 kDa to 30 kDa. However, at 60 kDa the dispersibility decreases notably, with large bundle-like structures appearing (Figure 1h). The poor dispersity of 60 kDa f-SWCNT may be related to the low grafting density (13.5 wt.%, Supplementary Figure S1a) or the large Flory radius [44] of the grafted polymer.

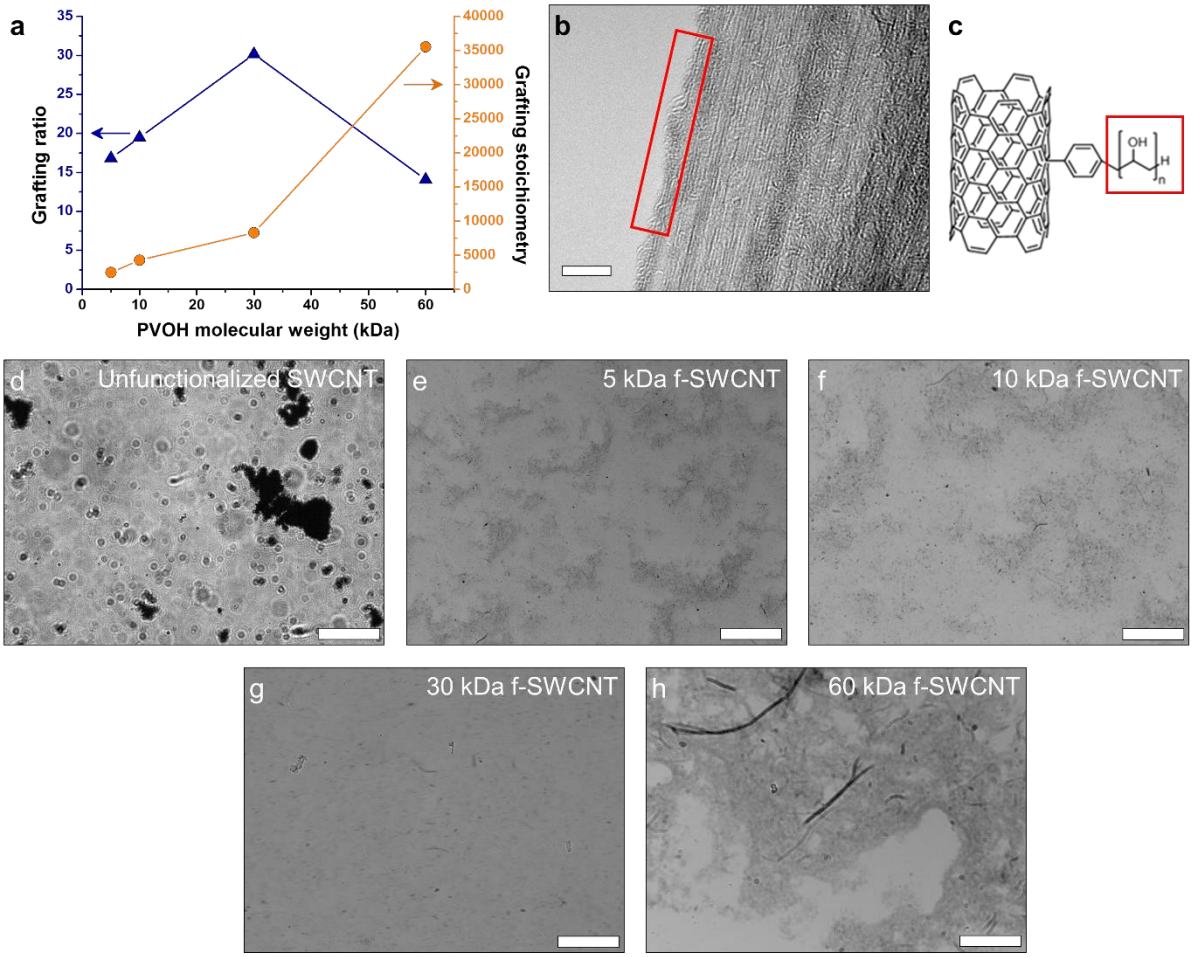

Figure 1 (a) Grafting ratio (weight fraction) of polymer and grafting stoichiometry (C/R) with differing PVOH chain lengths, (b) TEM image of 10 kDa f-SWCNTs, scale bar 5 nm, (c) schematic of PVOH functionalized on the side of a SWCNT. Optical micrographs of dispersions (d) unfunctionalized SWCNTs, and (e) to (h) f-SWCNTs in the dope solvent (DMSO/water 3:1 v/v), with scale bars 50 µm.

3.2 Composite fiber spinning

Dopes were prepared by simply mixing (f-)SWCNT dispersions with PVOH solutions and briefly sonicating (5 min, 150 W), and spun into an anti-solvent (acetone) coagulation bath. Previous studies have used PVOH solution as a coagulant bath for carbon nanotube dispersions [45] because unfunctionalized carbon nanotubes agglomerate readily in PVOH

solutions; indeed, in this work, agglomeration limited the unfunctionalized control samples to 3 wt.% SWCNTs. However, the PVOH-grafted SWCNTs formed stable spinning dopes even at 40 wt.% solids (absolute concentration 16 $mg_{(SWCNT)}$ mL^{-1}). The compatibility of the f-SWCNTs and the homopolymer PVOH provides better composition control and uniformity than the traditional approach. The fiber composition was adjusted, taking the grafting ratio into account, to maintain a constant proportion of SWCNTs to total PVOH. The process is shown schematically in Figure 2. After spinning into acetone, TGA showed that the resulting fibers approximately retained the SWCNT/PVOH ratio of the constituent dope, indicating that little homopolymer is lost during the spinning procedure (Supplementary Figure S1b).

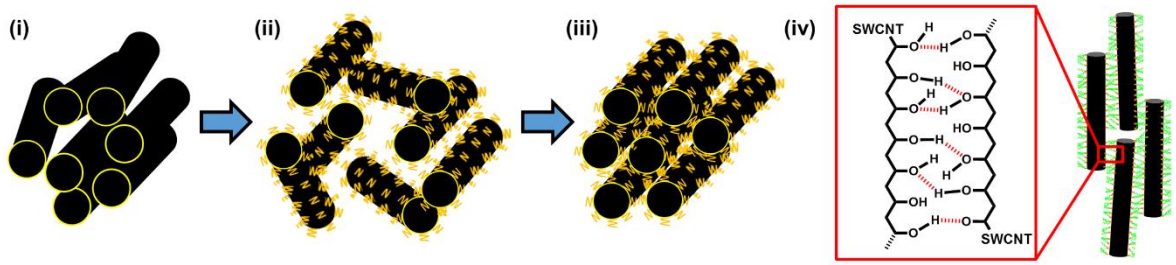

Figure 2 Schematic of fiber production. (i) Bundled SWCNTs, (ii) PVOH grafting to the SWCNT surface in a liquid phase, (iii) then the highly concentrated dispersion (dope) is wet spun into an anti-solvent coagulating into a SWCNT-PVOH composite fiber. (iv) Hydrogen bonding will form between f-SWCNTs in the composite fiber.

After removal from the coagulation bath, the fibers were subjected to a hot-drawing procedure (180 °C) to increase PVOH and SWCNT alignment, as well as PVOH crystallinity. As has been seen previously for multi-walled carbon nanotube/PVOH fibers [46], the treatment dramatically increased the strength and stiffness, while decreasing strain-to-failure (see discussion below, Figure 4b). The final f-SWCNT/PVOH composite fibers were ~50 m in length, (aside from 60 kDa f-SWCNT sample which broke during spinning, due to the poor dispersion), with a linear density of 0.8 ± 0.2 tex; the diameter of the fibers remained approximately similar across all the samples (~ 30 μm, Figure 3 and Supplementary Figure S3), and all fibers displayed a non-circular or ribbon-like cross-section. The SWCNT functionalization was critical for spinning and drawing composites with high filler loadings. The grafted PVOH improves compatibility with the matrix, reducing agglomeration, favoring alignment, and supporting the matrix above glass transition temperature (T_g); by encouraging load transfer, the f-SWCNTs strengthen the fiber during drawing.

3.3 Crystallinity of PVOH with f-SWCNT

The crystallinity of PVOH is increased by the hot drawing process that increases chain alignment [47]. Stiff fillers can also increase crystallinity by enhancing alignment or acting as nucleants [48]. Despite the surface constraint, grafted polymers can show accelerated crystallization kinetics, as found for multi-walled carbon nanotubes [49]. However, here, differential scanning calorimetry (DSC) (Supplementary Figure S4 and Supplementary Table S1) showed that the degree of crystallinity of pure PVOH ($\chi_{c(PVOH)}$ = 25.6%) modestly reduced with the addition of f-SWCNT (21.6 %, 24.6 %, and 19.1 % for 5 kDa, 10 kDa, and 30 kDa samples respectively). The decreases in crystallinity are largely consistent with the grafting of a relatively amorphous atactic polymer; however, the crystallinity of the homopolymer PVOH may also be disrupted by the shorter grafted polymer chains [50], which constitute a significant proportion of the total matrix.

3.4 SWCNT orientation and interface

High-resolution SEM micrographs of composite cryo-fractured cross-sections qualitatively suggest that most f-SWCNTs are preferentially aligned along the fiber axis (Figure 3 top). However, since reinforcement orientation is so critical to mechanical performance, especially of fibers, the orientation was quantified with both Raman spectroscopy and X-ray scattering measurements (Figure 3). First, polarized Raman maps were used to estimate the Herman parameter of the f-SWCNT parallel to the fiber axis. Briefly, the intensity of the G-mode (~1590 cm^{-1}) is highest when the incident laser is polarized parallel to the SWCNT axis (i.e. $\beta = 0°$) and the lowest when perpendicular (i.e. $\beta = 90°$) [51]. The Herman's orientation parameter (S) quantifies the degree of alignment, as a function of the angle between the nanotubes and the fiber axis (θ).

$$S = \frac{\langle 3\cos^2\theta \rangle - 1}{2} \quad (1)$$

For a random orientation of SWCNTs, $S = 0$ and for perfect orientation along the fiber axis, $S = 1$ [48, 51]. Assuming a uniaxial orientation, Raman data obtained with three different polarization configurations, I_{VV}, I_{VH}, and I_{HH}, where V and H refer to orientation parallel and perpendicular, respectively, can be used to estimate S:

$$S = \frac{3I_{VV} + I_{VH} - 4I_{HH}}{3I_{VV} + 12I_{VH} + 8I_{HH}} \quad (2)$$

The PVOH-grafted SWCNTs all show significant better alignment than the unfunctionalized SWCNT (3 wt.%) control sample (S= 0.23), maximized for the 10 kDa sample (S = 0.68). However, Raman measurements have a high spatial resolution but only probe the surface of the fiber. Bulk SWCNT alignment was confirmed by synchrotron SAXS and WAXS measurements (Figure 3 and Supplementary Figure S5 respectively), analyzed using procedures published previously [14]. In brief, in polymer-free carbon nanotube fibers, the azimuthal profiles determined from SAXS, which originate from the form factor and elongated bundle/pore structure, have been previously shown to be equivalent to the broad carbon nanotube (002) interplanar reflection [52] obtained from WAXS. The azimuthal profile obtained after radial integration of scattering intensity corresponds to the orientation distribution for SWCNTs, which is normal to the graphene basal planes for adjacent nanotubes and thus perpendicular to the nanotube main axis. The PVOH crystal orientation can be monitored through the $(10\bar{1})$ peak, relative both to the SWCNTs and the composite fiber axis. The SWCNT and PVOH orientation distribution functions for 10 kDa f-SWCNT/PVOH composite fibers (Supplementary Figure S5) overlap in WAXS, confirming that the alignment of the constituent parts are intrinsically linked. SAXS intensity in these systems, which lack long-range crystalline order, is much stronger than WAXS, and can be thus conveniently used to analyze individual 30-micron diameter composite fibers at short beam exposures without causing sample damage. To quantify the alignment, the SAXS data were integrated azimuthally to yield an azimuthal angular distribution with a characteristic full-width-half-maximum (FWHM). The trends (Fig. 3b-e (ii)) are consistent with the Raman data, showing significantly enhanced orientation for the f-SWCNT samples, with the best alignment for the 10 kDa fibers (narrow FWHM = 13.7°). The (bulk) SAXS FWHM showed a strong correlation with the (surface) Raman Herman parameter (Supplementary Figure S6), indicating that the nanotubes were indeed preferentially orientated to the nanocomposite fiber axis. The dramatically improved alignment observed for the grafted SWCNTs is consistent with the improved dispersion, since individualized SWCNTs facilitate reorientation during the hot-drawing.

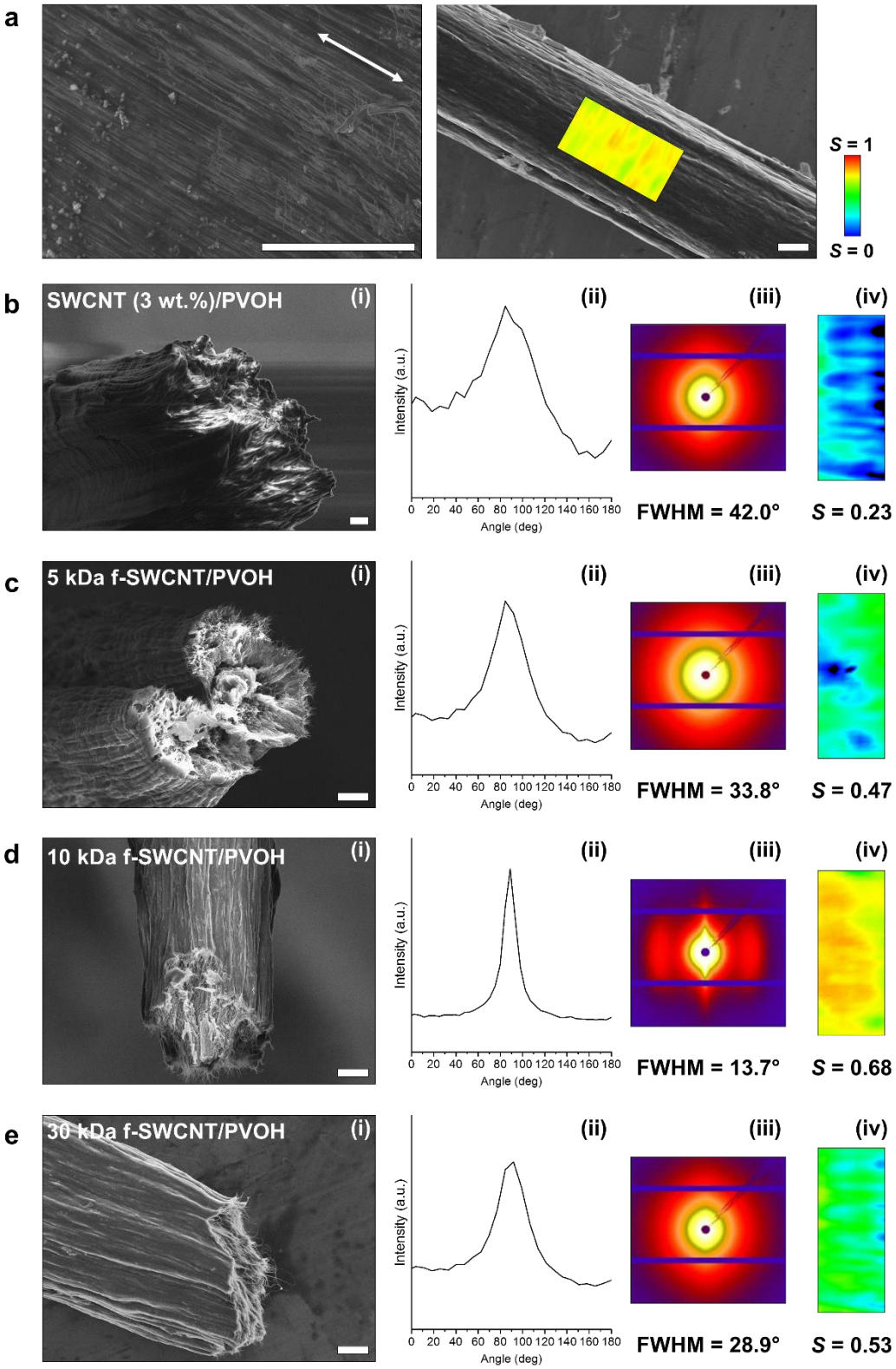

Figure 3 Composite fiber microscopy and SAXS patterns and polarized Raman spectroscopy analysis. (a) Left: SEM image of a 10 kDa f-SWCNT/PVOH composite fiber with a white arrow indicating the fiber axis; Right: A lower resolution image of the same fiber with a superimposed insert of a Herman orientation factor (*S*) Raman spectroscopy map. (b) Unfunctionalized SWCNT (3 wt.%) composite fiber (control); and (c), (d), and (e)

f-PVOH/PVOH composite fibers with M_w 5, 10, and 30 kDa, respectively. (i) SEM of cryo-fractured composite fiber surfaces; (ii) SAXS azimuthal curves and the corresponding (iii) 2D SAXS patterns with the full-width-at-half-maximum (FWHM) corresponding to the SWCNT alignment. Fiber axis horizontal; (iv) Herman's orientation parameter polarized Raman spectroscopy intensity map corresponding to surface SWCNT orientation. The scale bar is 5 μm for all frames. Micrographs of PVOH (100 wt.%) fiber and 60 kDa f-SWCNT/PVOH composite fiber in Supplementary Information, Figure S3.

3.5 Composite fiber properties

The mechanical properties for f-SWCNT/PVOH composite fibers were compared to PVOH (100 wt.%) fibers and unfunctionalized SWCNT (3 wt.%)/PVOH composite fibers (Figure 4, tabulated in Supplementary Table S2). Generally, the strength, stiffness, and toughness (fracture energy) of all the fibers improved on adding the f-SWCNTs to the PVOH, relative to the baseline fiber, with the exception of the 60 kDa f-SWCNTs system which suffered from obvious agglomeration (Figure 1h). Adding low levels of unfunctionalized SWCNTs increased strength (450 MPa) and modulus (14.8 GPa), modestly, but decreased strain-to-failure (7.1%) relative to the baseline matrix fibers (300 MPa strength, 7.7 GPa modulus, 12.8% strain-to-failure). In the f-SWCNT samples, the nanotube loading and intrinsic properties are constant, whilst the changes in matrix crystallinity are modest, hence the dramatically different mechanical response must be related to alignment and dispersion effects, induced by variations in the molecular weight of the grafted polymer. The improvement in performance, despite small reductions in matrix crystallinity indicate that the SWCNTs are directly contributing to reinforcement. The most oriented 10 kDa fiber has the highest strength and good stiffness, 1150 MPa and 24.0 GPa, respectively (an increase of 281% and 212%, respectively when compared to the PVOH baseline fiber); the excellent orientation allows the SWCNTs to be loaded effectively along the fiber axis. Although the 5 kDa fiber appears to have higher stiffness, despite the lower orientation, the difference is within experimental error. The length of the grafted polymer should determine the separation of the SWCNTs from the next reinforcing structure (whether another SWCNT or a PVOH crystallite). The fibers appear to yield at around 2% strain, presumably due to shear of the amorphous matrix between SWCNTs and PVOH crystals. When the PVOH grafted layer is thinner, the effective shear load is higher, leading to the steeper yield curve for the 5 kDa sample; as it becomes thicker, shear yielding becomes easier, eventually leading to the large strain-to-failure (ca. 23%) observed for the 30 kDa fiber which also demonstrated the highest toughness (126 J g^{-1}). The intermediate 10 kDa fiber combines a high yield strength with

large strain to failure, also leading to a high toughness (74 J g^{-1}). The nanocomposite fibers produced here have similar tensile properties to literature examples based on aerogel-synthesized carbon nanotubes in a PVOH matrix which have tensile strength ca. 1000-1200 MPa and stiffness ca. 24-30 GPa, but lower toughness due to a lower strain-to-failure (ca. 9%) [17]. The 10 kDa f-SWCNT/PVOH fibers also compare well with wet-spun ester linked nanocomposite fibers, with ~5 wt.% SWCNT loading [53]. The ester-linked fibers exhibited lower tensile strength ca. 325 MPa and stiffness ca. 22 GPa, but due to a very high strain-to-failure (~200%) exhibited a higher toughness (400 J g^{-1}). Current state-of-the-art PVOH nanocomposite fiber systems, with controlled polymer crystallization during gel-spinning and small diameters (10 wt.%, ca. 10 μm diameter [54]) and higher-SWCNT concentration (60 wt.% [55]), have better performance, and indicate the scope to enhance the performance of the new grafted-SWCNT nanocomposite system further.

An additional figure of merit for these moderate modulus and high fracture toughness fibers is to compare their ballistic protection capacity, $U^{1/3}$, the product of the acoustic wave speed and the cube-root of the specific fracture energy, discussed in detail elsewhere [14, 56, 57]). F-SWCNT/PVOH fibers have an average $U^{1/3}$ between ca. 250 and ca. 600 m s^{-1}, which increased on increasing f-SWCNT polymer chain length (omitting 60 kDa); composite fiber bulk densities were estimated at 1.29 ± 1 g cm^{-1}, using material densities for amorphous PVOH, crystalline PVOH [58], and SWCNTs [59] of 1.269 g cm^{-3}, 1.345 g cm^{-3}, and 1.3 g cm^{-3}, respectively (Supplementary Table S2). The highest f-SWCNT/PVOH composite ballistic protection performance was comparable to commercial E-glass fibers and carbon fibers (560 and 590 m s^{-1}, respectively) [56].

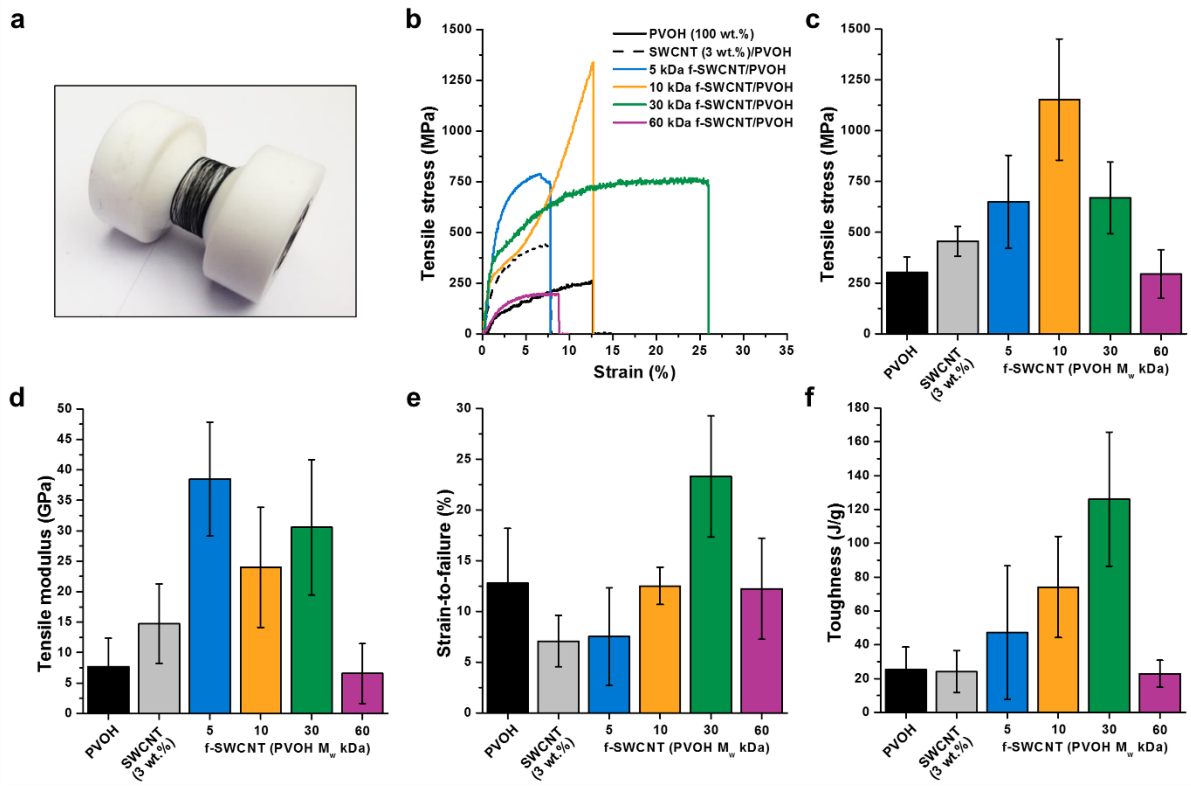

Figure 4 Mechanical tensile properties of f-SWCNT/PVOH composite fibers compared with PVOH (100 wt.%, matrix only) fiber and unfunctionalized SWCNT (3 wt.%)/PVOH composite fiber (control). (a) A photograph of f-SWCNT/PVOH composite fiber collected on a winder (10 m in length), (b) typical stress-strain curves, (c) ultimate tensile strength. (d) tensile modulus, (e) strain-to-failure, (f) tensile toughness (energy of deformation). The error bars represent standard deviation and individual stress-strain curves provided in the Supplementary Figure S7 and Figure S8.

4. Conclusions

In summary, well-defined polymers, with a range of molecular weights, were grafted to SWCNTs in order to improve the microstructure of nanoreinforced PVOH fibers. The grafting improves dispersion and enables coagulation spinning of nanocomposite fibers with a high loading fraction of SWCNTs. By preparing a spinning dope that combines the homopolymer matrix and the reinforcement, homogeneous fibers were formed with a well-defined composition. Well dispersed, individualized SWCNTs align readily during spinning and subsequent drawing, improving the mechanical properties of the composite fibers. However, the molecular weight of the grafted polymer determines the yielding behavior. This rational strategy for enhancing load capacity via nanotube reinforcement,

whilst modulating the yield behavior by defined grafting, provides a promising avenue for the long standing materials challenge of optimizing strength, stiffness, and toughness simultaneously. The best PVOH grafted SWCNT/PVOH fibers obtained so far (10 kDa) combined high stiffness (24 GPa), strength (1100 MPa) and strain-to-failure (12.5%) allowing access to high toughnesses (74 J g^{-1}). Interfacial control is clearly critical in nanocomposites, in which interphase dominates; proper design is essential not only for SWCNTs but also in other 1D nanoreinforced systems. In the current study, homopolymer PVOH is used to improve the spinnability of the grafted SWCNTs; however, there is significant scope to improve performance further, once grafting, grafted polymer tacticity, nanomaterial aspect ratio, and processing are all optimized. Ultimately, designed systems consisting only of grafted nanomaterials can be expected to offer improved properties.

Supplementary Information

Thermogravimetric analysis thermograms, additional microscopy images, additional tensile stress-strain curves, differential scanning calorimetry profiles, and orientation distribution functions curves from SAXS are available in supplementary information.

Declaration

The authors declare no competing financial interest.

Author Contributions

W.J.L., A.J.C., F.C.F.T., J.J.V. and M.S.P.S. designed the study. W.J.L., A.J.C., and D.B.A., carried out the composite fiber fabrication and mechanical testing and other characterization detailed in the manuscript. E.R.W and H.S.L. carried out the transmission electron microscopy characterization. F.C.F.T. and E.S. carried out the X-ray scattering experiments. F.C.F.T. and J.J.V. preformed the analysis of the X-ray scattering data. W.J.L. and A.J.C. wrote the first version of the manuscript, and all authors participated in manuscript writing/editing and contributed to the data interpretation. All authors have given approval to the final version of the manuscript. W.J.L. and A.J.C. have contributed equally.

Acknowledgement

We are grateful to Dr. Andreas Mautner and Prof. Alexander Bismarck (University of Vienna) for their help using the DSM Xplore Fiber Conditioning Unit. The authors would like to thank the European Union Seventh Framework Program under grant agreement 678565 (ERC-STEM) and The Engineering and Physical Sciences Research Council (EPSRC Programme Grant EP/I02946X/1) for financial support as part of the High Performance Ductile Composite Technology (HiPerDuCT) Project in collaboration with University of Bristol. The SAXS-WAXS experiments were performed at NCD-SWEET beamline at ALBA synchrotron with the collaboration of ALBA staff. Supporting data can be requested from the corresponding author but may be subject to confidentiality obligations.

References

[1] V.C. Li, H.-C. Wu, Conditions for Pseudo Strain-Hardening in Fiber Reinforced Brittle Matrix Composites, Applied Mechanics Reviews 1992; 45(8):390-398. http://doi.org/10.1115/1.3119767
[2] W.J. Cantwell, J. Morton, The Significance of Damage and Defects and Their Detection in Composite Materials: A Review, The Journal of Strain Analysis for Engineering Design 1992; 27(1):29-42. http://doi.org/10.1243/03093247v271029
[3] G. Czél, M. Jalalvand, M.R. Wisnom, Hybrid Specimens Eliminating Stress Concentrations in Tensile and Compressive Testing of Unidirectional Composites, Composites Part A: Applied Science and Manufacturing 2016; 91:436-447. http://doi.org/10.1016/j.compositesa.2016.07.021
[4] G. Czél, M. Jalalvand, M.R. Wisnom, T. Czigány, Design and Characterisation of High Performance, Pseudo-Ductile All-Carbon/Epoxy Unidirectional Hybrid Composites, Composites Part B: Engineering 2017; 111:348-356. http://doi.org/10.1016/j.compositesb.2016.11.049
[5] L. Feng, K. Li, B. Xue, Q. Fu, L. Zhang, Optimizing Matrix and Fiber/Matrix Interface to Achieve Combination of Strength, Ductility and Toughness in Carbon Nanotube-Reinforced Carbon/Carbon Composites, Materials & Design 2017; 113:9-16. http://doi.org/10.1016/j.matdes.2016.10.006
[6] V.N. Popov, V.E. Van Doren, M. Balkanski, Elastic Properties of Single-Walled Carbon Nanotubes, Physical Review B 2000; 61(4):3078-3084. http://doi.org/10.1103/PhysRevB.61.3078
[7] T.W. Odom, J.-L. Huang, P. Kim, C.M. Lieber, Atomic Structure and Electronic Properties of Single-Walled Carbon Nanotubes, Nature 1998; 391:62. http://doi.org/10.1038/34145
[8] J.N. Coleman, U. Khan, W.J. Blau, Y.K. Gun'ko, Small but Strong: A Review of the Mechanical Properties of Carbon Nanotube–Polymer Composites, Carbon 2006; 44(9):1624-1652. http://doi.org/10.1016/j.carbon.2006.02.038
[9] Y. Liu, S. Kumar, Polymer/Carbon Nanotube Nano Composite Fibers–a Review, ACS applied materials & interfaces 2014; 6(9):6069-6087. http://doi.org/10.1021/am405136s
[10] K. Song, Y. Zhang, J. Meng, E. Green, N. Tajaddod, H. Li, M. Minus, Structural Polymer-Based Carbon Nanotube Composite Fibers: Understanding the Processing–Structure–Performance Relationship, Materials 2013; 6(6):2543. http://www.mdpi.com/1996-1944/6/6/2543
[11] A.A. Kuznetsov, A.F. Fonseca, R.H. Baughman, A.A. Zakhidov, Structural Model for Dry-Drawing of Sheets and Yarns from Carbon Nanotube Forests, ACS Nano 2011; 5(2):985-993. http://doi.org/10.1021/nn102405u
[12] T.S. Gspann, F.R. Smail, A.H. Windle, Spinning of Carbon Nanotube Fibres Using the Floating Catalyst High Temperature Route: Purity Issues and the Critical Role of Sulphur, Faraday Discussions 2014; 173(0):47-65. http://doi.org/10.1039/C4FD00066H
[13] K. Koziol, J. Vilatela, A. Moisala, M. Motta, P. Cunniff, M. Sennett, A. Windle, High-Performance Carbon Nanotube Fiber, Science 2007; 318(5858):1892-1895. http://doi.org/10.1126/science.1147635
[14] J.C. Fernández-Toribio, B. Alemán, Á. Ridruejo, J.J. Vilatela, Tensile Properties of Carbon Nanotube Fibres Described by the Fibrillar Crystallite Model, Carbon 2018; 133:44-52. http://doi.org/10.1016/j.carbon.2018.03.006
[15] M.L. Wu, Y. Chen, L. Zhang, H. Zhan, L. Qiang, J.N. Wang, High-Performance Carbon Nanotube/Polymer Composite Fiber from Layer-by-Layer Deposition, ACS applied materials & interfaces 2016; 8(12):8137-8144. http://doi.org/10.1021/acsami.6b01130
[16] Y. Jung, T. Kim, C.R. Park, Effect of Polymer Infiltration on Structure and Properties of Carbon Nanotube Yarns, Carbon 2015; 88:60-69. http://doi.org/10.1016/j.carbon.2015.02.065
[17] J. Liu, W. Gong, Y. Yao, Q. Li, J. Jiang, Y. Wang, G. Zhou, S. Qu, W. Lu, Strengthening Carbon Nanotube Fibers with Semi-Crystallized Polyvinyl Alcohol and Hot-Stretching, Composites Science and Technology 2018; 164:290-295. http://doi.org/10.1016/j.compscitech.2018.06.003
[18] P.M. Ajayan, J.M. Tour, Nanotube Composites, Nature 2007; 447:1066. http://doi.org/10.1038/4471066a
[19] L. Henrard, E. Hernández, P. Bernier, A. Rubio, Van Der Waals Interaction in Nanotube Bundles: Consequences on Vibrational Modes, Physical Review B 1999; 60(12):R8521-R8524. http://doi.org/10.1103/PhysRevB.60.R8521

[20] E.T. Thostenson, Z. Ren, T.-W. Chou, Advances in the Science and Technology of Carbon Nanotubes and Their Composites: A Review, Composites Science and Technology 2001; 61(13):1899-1912. http://doi.org/10.1016/S0266-3538(01)00094-X
[21] K.M. Liew, C.H. Wong, M.J. Tan, Tensile and Compressive Properties of Carbon Nanotube Bundles, Acta Materialia 2006; 54(1):225-231. http://doi.org/10.1016/j.actamat.2005.09.002
[22] Y.S. Song, J.R. Youn, Influence of Dispersion States of Carbon Nanotubes on Physical Properties of Epoxy Nanocomposites, Carbon 2005; 43(7):1378-1385. http://doi.org/10.1016/j.carbon.2005.01.007
[23] T.H. Lim, S.H. Lee, S.Y. Yeo, Highly Conductive Polymer/Metal/Carbon Nanotube Composite Fiber Prepared by the Melt-Spinning Process, Textile Research Journal 2016; 87(5):593-606. http://doi.org/10.1177/0040517516632481
[24] L. Ericson, H. Fan, H. Peng, V. Davis, W. Zhou, J. Sulpizio, Y. Wang, R. Booker, J. Vavro, C. Guthy, A. Parra-Vasquez, M. Kim, S. Ramesh, R. Saini, C. Kittrell, G. Lavin, H. Schmidt, W. Adams, W. Billups, M. Pasquali, W.-F. Hwang, R. Hauge, J. Fischer, R. Smalley, Macroscopic, Neat, Single-Walled Carbon Nanotube Fibers, Science 2004; 305(5689):1447-1450. http://doi.org/10.1126/science.1101398
[25] C. Jiang, A. Saha, C. Xiang, C.C. Young, J.M. Tour, M. Pasquali, A.A. Martí, Increased Solubility, Liquid-Crystalline Phase, and Selective Functionalization of Single-Walled Carbon Nanotube Polyelectrolyte Dispersions, ACS Nano 2013; 7(5):4503-4510. http://doi.org/10.1021/nn4011544
[26] A.J. Clancy, M.K. Bayazit, S.A. Hodge, N.T. Skipper, C.A. Howard, M.S.P. Shaffer, Charged Carbon Nanomaterials: Redox Chemistries of Fullerenes, Carbon Nanotubes, and Graphenes, Chemical Reviews 2018. http://doi.org/10.1021/acs.chemrev.8b00128
[27] A.J. Clancy, D.B. Anthony, S.J. Fisher, H.S. Leese, C.S. Roberts, M.S.P.S. Shaffer, Reductive Dissolution of Supergrowth Carbon Nanotubes for Tougher Nanocomposites by Reactive Coagulation Spinning, Nanoscale 2017; 9(25):8764-8773. http://doi.org/10.1039/c7nr00734e
[28] Y. Martinez-Rubi, B. Ashrafi, J. Guan, C. Kingston, A. Johnston, B. Simard, V. Mirjalili, P. Hubert, L. Deng, R. Young, Toughening of Epoxy Matrices with Reduced Single-Walled Carbon Nanotubes, ACS applied materials & interfaces 2011; 3(7):2309-2317. http://doi.org/10.1021/am200523z
[29] M.M.E. Jacob, A.K. Arof, Ftir Studies of Dmf Plasticized Polyvinyledene Fluoride Based Polymer Electrolytes, Electrochimica Acta 2000; 45(10):1701-1706. http://doi.org/10.1016/S0013-4686(99)00316-3
[30] A. Hirsch, Functionalization of Single-Walled Carbon Nanotubes, Angewandte Chemie-International Edition 2002; 41(11):1853-1859. http://doi.org/10.1002/1521-3773(20020603)41:11<1853::AID-ANIE1853>3.0.CO;2-N
[31] B. Vigolo, V. Mamane, F. Valsaque, T.N.H. Le, J. Thabit, J. Ghanbaja, L. Aranda, Y. Fort, E. Mcrae, Evidence of Sidewall Covalent Functionalization of Single-Walled Carbon Nanotubes and Its Advantages for Composite Processing, Carbon 2009; 47(2):411-419. http://doi.org/10.1016/j.carbon.2008.10.024
[32] J. Zhu, J. Kim, H. Peng, J.L. Margrave, V.N. Khabashesku, E.V. Barrera, Improving the Dispersion and Integration of Single-Walled Carbon Nanotubes in Epoxy Composites through Functionalization, Nano Letters 2003; 3(8):1107-1113. http://doi.org/10.1021/nl0342489
[33] C. Fu, L. Gu, Composite Fibers from Poly(Vinyl Alcohol) and Poly(Vinyl Alcohol)-Functionalized Multiwalled Carbon Nanotubes, Journal of Applied Polymer Science 2013; 128(2):1044-1053. http://doi.org/10.1002/app.38260
[34] Z. Yao, N. Braidy, G.A. Botton, A. Adronov, Polymerization from the Surface of Single-Walled Carbon Nanotubes − Preparation and Characterization of Nanocomposites, Journal of the American Chemical Society 2003; 125(51):16015-16024. http://doi.org/10.1021/ja037564y
[35] R.C. Chadwick, U. Khan, J.N. Coleman, A. Adronov, Polymer Grafting to Single-Walled Carbon Nanotubes: Effect of Chain Length on Solubility, Graft Density and Mechanical Properties of Macroscopic Structures, Small 2013; 9(4):552-60. http://doi.org/10.1002/smll.201201683

[36] P. Zhang, D. Qiu, H. Chen, J. Sun, J. Wang, C. Qin, L. Dai, Preparation of Mwcnts Grafted with Polyvinyl Alcohol through Friedel–Crafts Alkylation and Their Composite Fibers with Enhanced Mechanical Properties, Journal of Materials Chemistry A 2015; 3(4):1442-1449. http://doi.org/10.1039/C4TA03979C
[37] A.J. Clancy, J.M. Serginson, J.L. Greenfield, M.S.P. Shaffer, Systematic Comparison of Single-Walled Carbon Nanotube/Poly(Vinyl Acetate) Graft-to Reactions, Polymer 2017; 133:263-271. http://doi.org/10.1016/j.polymer.2017.10.047
[38] M. Basham, J. Filik, M.T. Wharmby, P.C.Y. Chang, B. El Kassaby, M. Gerring, J. Aishima, K. Levik, B.C.A. Pulford, I. Sikharulidze, D. Sneddon, M. Webber, S.S. Dhesi, F. Maccherozzi, O. Svensson, S. Brockhauser, G. Naray, A.W. Ashton, Data Analysis Workbench (Dawn), Journal of Synchrotron Radiation 2015; 22(3):853-858. http://doi.org/10.1107/S1600577515002283
[39] R.K. Tubbs, Melting Point and Heat of Fusion of Poly(Vinyl Alcohol), Journal of Polymer Science Part A: General Papers 1965; 3(12):4181-4189. http://doi.org/10.1002/pol.1965.100031213
[40] A.J. Clancy, J. Melbourne, M.S. Shaffer, A One-Step Route to Solubilised, Purified or Functionalised Single-Walled Carbon Nanotubes, Journal of Materials Chemistry A 2015; 3(32):16708-16715. http://doi.org/10.1039/c5ta03561a
[41] S. Qin, D. Qin, W.T. Ford, D.E. Resasco, J.E. Herrera, Functionalization of Single-Walled Carbon Nanotubes with Polystyrene Via Grafting to and Grafting from Methods, Macromolecules 2004; 37(3):752-757. http://doi.org/10.1021/ma035214q
[42] S.N. Ushakov, T.A. Kononova, Synthesis of Esters of Polyvinyl Alcohol, Bulletin of the Academy of Sciences of the USSR, Division of chemical science 1955; 4(1):103-108. http://doi.org/10.1007/bf01177515
[43] A.J. Clancy, E.R. White, H.H. Tay, H.C. Yau, M.S.P. Shaffer, Systematic Comparison of Conventional and Reductive Single-Walled Carbon Nanotube Purifications, Carbon 2016; 108:423-432. http://doi.org/10.1016/j.carbon.2016.07.034
[44] P.G. De Gennes, Conformations of Polymers Attached to an Interface, Macromolecules 1980; 13(5):1069-1075. http://doi.org/10.1021/ma60077a009
[45] C. Mercader, A. Lucas, A. Derré, C. Zakri, S. Moisan, M. Maugey, P. Poulin, Kinetics of Fiber Solidification, Proceedings of the National Academy of Sciences 2010; 107(43):18331-18335. http://doi.org/10.1073/pnas.1003302107
[46] P. Miaudet, S. Badaire, M. Maugey, A. Derre, V. Pichot, P. Launois, P. Poulin, C. Zakri, Hot-Drawing of Single and Multiwall Carbon Nanotube Fibers for High Toughness and Alignment, Nano Letters 2005; 5(11):2212-2215. http://doi.org/10.1021/nl051419w
[47] S. Lee, W. Sung, Coil-to-Stretch Transition, Kink Formation, and Efficient Barrier Crossing of a Flexible Chain, Physical Review E 2001; 63(2):021115. http://doi.org/10.1103/PhysRevE.63.021115
[48] W. Lee, A.J. Clancy, E. Kontturi, A. Bismarck, M. Shaffer, Strong and Stiff: High Performance Cellulose Nanocrystal/Polyvinyl Alcohol Composite Fibers, ACS applied materials & interfaces 2016. http://doi.org/10.1021/acsami.6b11578
[49] D. Baskaran, J.W. Mays, M.S. Bratcher, Polymer-Grafted Multiwalled Carbon Nanotubes through Surface-Initiated Polymerization, Angewandte Chemie International Edition 2004; 43(16):2138-2142. http://doi.org/10.1002/anie.200353329
[50] N.S. Alghunaim, Optimization and Spectroscopic Studies on Carbon Nanotubes/Pva Nanocomposites, Results in Physics 2016; 6:456-460. http://doi.org/10.1016/j.rinp.2016.08.002
[51] E. Brandley, E.S. Greenhalgh, M.S.P. Shaffer, Q. Li, Mapping Carbon Nanotube Orientation by Fast Fourier Transform of Scanning Electron Micrographs, Carbon 2018; 137:78-87. http://doi.org/10.1016/j.carbon.2018.04.063
[52] Z.Q. Li, C.J. Lu, Z.P. Xia, Y. Zhou, Z. Luo, X-Ray Diffraction Patterns of Graphite and Turbostratic Carbon, Carbon 2007; 45(8):1686-1695. http://doi.org/10.1016/j.carbon.2007.03.038
[53] J.M. González-Domínguez, W. Neri, M. Maugey, P. Poulin, A. Ansón-Casaos, M. Teresa Martínez, A Chemically Reactive Spinning Dope for Significant Improvements in Wet Spun Carbon Nanotube Fibres, Chemical Communications 2013; 49(38):3973-3975. http://doi.org/10.1039/c3cc38953g

[54] J. Meng, Y. Zhang, K. Song, M.L. Minus, Forming Crystalline Polymer-Nano Interphase Structures for High-Modulus and High-Tensile/Strength Composite Fibers, Macromolecular Materials and Engineering 2014; 299(2):144-153. http://doi.org/10.1002/mame.201300025
[55] A.B. Dalton, S. Collins, E. Munoz, J.M. Razal, V.H. Ebron, J.P. Ferraris, J.N. Coleman, B.G. Kim, R.H. Baughman, Super-Tough Carbon-Nanotube Fibres, Nature 2003; 423(6941):703-703. http://doi.org/10.1038/423703a
[56] P.M. Cunniff, M.A. Auerbach, E. Vetter, D.J. Sikkema, High Performance "M5" Fiber for Ballistics/Structural Composites, 23rd. Army Science Conference Assistant Secretary of the Army (Acquisition, Logistics and Technology), Orlando, Florida, 2002. http://stuff.mit.edu/afs/athena/course/3/3.91/www/slides/cunniff.pdf
[57] G.A. Holmes, K. Rice, C.R. Snyder, Ballistic Fibers: A Review of the Thermal, Ultraviolet and Hydrolytic Stability of the Benzoxazole Ring Structure, J Mater Sci 2006; 41(13):4105-4116. http://doi.org/10.1007/s10853-005-5597-1
[58] N.A. Peppas, E.W. Merrill, Poly(Vinyl Alcohol) Hydrogels: Reinforcement of Radiation-Crosslinked Networks by Crystallization, Journal of Polymer Science: Polymer Chemistry Edition 1976; 14(2):441-457. http://doi.org/10.1002/pol.1976.170140215
[59] M. Meyyappan, Carbon Nanotubes: Science and Applications, CRC Press, Florida, 2004, p. 289. http://www.crcpress.com/Carbon-Nanotubes-Science-and-Applications/Meyyappan/p/book/9780849321115

Acronyms and symbols

β, incident laser angle in relation to the SCWNT fiber axis
C/R, SWCNT carbons per polymer chain/grafting ratio
DCM, dichloromethane
DMAc, N,N-dimethylacetamide
DMSO, dimethyl sulfoxide
DSC, differential scanning calorimetry
LPE, liquid phase exfoliation
f-SWCNT, functionalized single-walled carbon nanotube
FWHM, full width at half maximum
H, polarization orientation perpendicular
$M_{n,}$ average molar mass
NCD, non-crystalline diffraction
PTFE, polytetrafluoroethylene
PVOH, polyvinyl alcohol
PVAc, acyl-protected polyvinyl acetate
RAFT, reversible addition–fragmentation chain transfer
S, Herman orientation order parameter
SEM, scanning electron microscopy
SAXS, small angle two-dimensional X-ray scattering
SWCNT, single-walled carbon nanotube
TEM, transmission electron microscopy
T_g, glass transition temperature
TGA, thermogravimetric analysis
θ, angle between the nanotubes and the fiber axis
THF, tetrahydrofuran
$U^{1/3}$, ballistic protection
V, polarization orientation parallel
χ_c, degree of crystallinity